

pubs.acs.org/JPCC Article

In-Situ Oxygen Isotopic Exchange Vibrational Spectroscopy of Rhenium Oxide Surface Structures on Cerium Oxide

Blake MacQueen, Benjamin Ruiz-Yi, Michael Royko, Andreas Heyden, Yomaira J. Pagan-Torres, Christopher Williams, and Jochen Lauterbach*

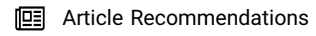


Cite This: J. Phys. Chem. C 2020, 124, 7174-7181



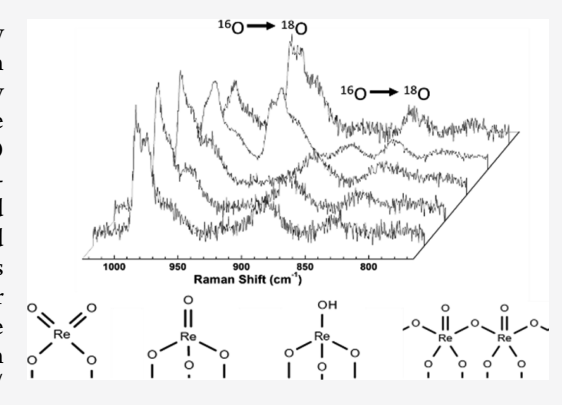
ACCESS I

Metrics & More



SI Supporting Information

ABSTRACT: The surface structures of ReO_x supported on CeO_2 at low loadings have been elucidated through ^{18}O isotopic exchange Raman spectroscopy and diffuse reflectance infrared Fourier transform spectroscopy (DRIFTS). The ReO_x is present in four distinct structures, a di-oxo structure with two Re=O terminal bonds, a mono-oxo species that contains one Re=O terminal bond, a mono-oxo species that contains a hydroxyl group, and a cross-linked ReO_x species. The isotopic exchange Raman spectroscopy shows a red shift resulting from the ^{18}O exchange in the O=Re=O, Re=O, Re=OH, and Re-O-Re species, which allowed for the deconvolution of the various structures. Time-resolved DRIFTS showed significant exchange of ^{18}O over time and reconfirmed the results from the Raman spectroscopy. The presence of multiple surface species supports the existence of competing reaction mechanisms for the simultaneous hydrodeoxygenation over the ReO_x-Pd/CeO_2 catalyst and deoxydehydration over the ReO_x/CeO_2 catalyst.



■ INTRODUCTION

The surface structure of ReO_x supported on CeO_2 has not been confirmed in detail via vibrational spectroscopic methods and is currently debated in the literature. Several theoretical studies^{1,2} suggest that there are three likely structures that the isolated monomeric ReO_x species could form: mono-oxo, dioxo, and tri-oxo, as shown in Figure 1.

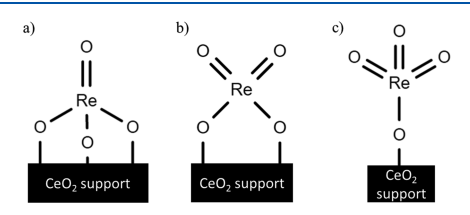


Figure 1. Structures of isolated Re sites in ReO_x/CeO_2 catalyst. (a) Mono-oxo structure. (b) Di-oxo structure. (c) Tri-oxo structure.

The structures shown in Figure 1 are for isolated monomeric Re sites that can be present in submonolayer coverages of Re on CeO₂. Once the Re weight loading increases, the possibility for the formation of an oligomeric cross-linked structure increases. The CeO₂ typically has a surface area between 80 and 150 m²/g, which depends on the synthesis method and post treatment. The theoretical total number of Re sites that can be occupied on the CeO₂ corresponds to a 20 wt % loading of Re. However, cross-linking has been experimentally observed in 3 wt % Re₂O₇/ZrO₂¹¹ as well as proposed for 2 wt

% ReO_x-Pd/CeO_{2.} In order to reduce the possibility of having cross-linkage and to maximize the amount of isolated Re sites, a relatively low weight loading of 1 wt % (nominal) Re on CeO₂ was chosen for this study. This loading would also allow us to spectroscopically monitor the Re=O bonds with a sufficient signal-to-noise ratio during isotopic exchange experiments.

Isotope exchange is a common technique used in conjunction with vibrational spectroscopy techniques as a means of identifying the number and types of vibrations in a material system. ^{12–16} Within the literature, there have been multiple isotope exchange experiments performed on ReO_x on various supports such as Al₂O₃, ZrO₂, TiO₂, Cr₂O₃, and SiO₂ to determine the speciation of the ReO_x on the surface. ^{11,12,17–19} However, the same set of experiments has not been performed on CeO₂ supports. These experiments, in conjunction with previous information on the ReO_x vibrational modes, ^{20,21} show the speciation of the catalyst from the number of bands that appear post-isotope exchange. With respect to the potential ReO_x species seen in Figure 1, the mono-oxo could show two bands post isotope exchange

Received: December 6, 2019 Revised: February 12, 2020 Published: March 11, 2020



(stretching of Re= 16 O and Re= 18 O), the di-oxo has six bands (symmetric and asymmetric stretching of ¹⁶O=Re=¹⁶O, $^{18}O = \text{Re} = ^{16}O$, and $^{18}O = \text{Re} = ^{18}O$), and the tri-oxo has eight bands (symmetric and asymmetric stretching of the $^{16}O = Re(=^{16}O) = ^{16}O, \quad ^{18}O = Re(=^{16}O) = ^{16}O \quad ^{18}O = Re$ $(=^{18}O)=^{16}O$, and $^{18}O=Re(=^{18}O)=^{18}O$). However, it has been shown that multiple different species can form on the surface instead of any one speciation, leading to increasing complexity of the spectral analysis post-exchange. Andriopoulou and Boghosian showed mono-oxo and di-oxo configurations of ReO_r on TiO₂ at 350 °C. 19 Additionally, Weckhuysen et al. showed that mono-oxo metal oxide species co-exist with cross-linked metal oxide species on a ZrO₂ support. 11 Thus, any single or co-existing monomeric or oligomeric ReO_x species can be determined through isotopic exchange vibrational spectroscopy experimentation.

ReO_x/CeO₂ holds significant value in its superior ability to remove oxygen-containing groups from various compounds through deoxydehydration $(DODH)^{22-28}$ and through hydrodeoxygenation (HDO) when supported with Pd. 1,29,30 ReO.-Pd/CeO₂ is the state-of-the-art catalyst for the simultaneous hydrodeoxygenation (S-HDO) of sugar alcohols in which two vicinal hydroxyl groups are removed at the same time. 1,29,30 The S-HDO is comprised of two steps, a DODH step followed by a hydrogenation step. The ReO_x/CeO₂ is responsible for the DODH step and has been utilized for a variety of substrates such as glycerol, 1,4-anhydroerythritol, and methyl glycosides. 22-28 The palladium catalyzes hydrogen dissociation and is responsible for hydrogen spillover onto the surface, which promotes the hydrogenation step.² A previously proposed reaction mechanism by Ota et al. for the ReO_x-Pd/CeO₂-catalyzed S-HDO starts with an isolated Re^{VI} species. This theoretical study used Re atoms randomly dispersed among all of the possible sites of a Ce₇₀O₁₄₀, CeO₂ (1 1 1), (87 m² g⁻¹) support surface. The S-HDO reaction mechanism calculated from the density functional theory (DFT) starts with tri-oxo species, shown in Figure 1c, which is then reduced to a di-oxo structure, shown in Figure 1b, which changes the oxidation state from Re^{IV} to Re^{VI} species once the 1,4-anhydroerythritol attaches to the ReO_x. The resulting Re^{VI} species remains di-oxo but has one Re-O bond from the CeO₂, two terminal Re=O bonds, and two Re-O bonds from the substrate. The reduction from the Re^{VI} to Re^{IV} was proposed to be promoted by the Pd on the catalyst. After forming the di-oxo species with the 1,4-anhydroerythritol attached, the S-HDO is proposed to occur via the DODH followed by the hydrogenation of the alkene. The ReO_x species is in a tri-oxo structure after the formed tetrahydrofuran (THF) desorbs but is then reduced back to the di-oxo structure, which is catalyzed by the Pd, resulting in a regenerative cycle.

Another reported mechanism by Xi et al.² has the isolated Re species starting as a mono-oxo structure with one terminally double-bonded oxygen atom and three single-bonded oxygen atoms that are bonded to the ceria support, see Figure 1a. This study utilized a fully hydroxylated CeO₂ (1 1 1) support surface with four O–Ce–O trilayers, which resulted in the mono-oxo structure being the most energetically favorable structure under reaction conditions.² After the 1,4-anhydroerythritol adsorbs, the DODH then occurs, leaving the Re species in a di-oxo structure, which is then reduced back to the mono-oxo structure through a regenerative hydrogen migration process.² The starting surface structure of the Re in the

reaction mechanism differs in the DFT calculations in the literature, which results in varying proposed mechanisms for the S-HDO. ^{1,2}

Since both DFT studies suggest different starting structures, the resulting proposed reaction mechanisms also vary. However, each calculated mechanism predicts differing regeneration cycles that include a specific isolated ${\rm ReO}_x$ surface structure on which the sugar alcohol adsorbs. In order to experimentally confirm the surface structure of ${\rm ReO}_x$ on ${\rm CeO}_2$ and gain insight into the starting point of the reaction mechanism, this work utilized in situ isotopic oxygen exchange experiments in combination with Raman spectroscopy and diffuse reflectance infrared Fourier transform spectroscopy (DRIFTS).

EXPERIMENTAL SECTION

Chemicals. Cerium (IV) oxide, ammonium perrhenate, and oxygen- $^{18}O_2$ isotope were used in this work. The cerium (IV) oxide CAS no. 1306-38-3 was supplied by Daiichi Kigenso Kagaku Kogyo Co., Ltd. The ammonium perrhenate of ≥99% purity, CAS no. 13598-5-7, and the oxygen− $^{18}O_2$ isotope of 99% purity, CAS no. 32767-18-3, were obtained from Sigma-Aldrich.

 $\mbox{ReO}_x/\mbox{CeO}_2$ Synthesis. The $\mbox{ReO}_x/\mbox{CeO}_2$ catalysts were prepared using the method previously described by Ota et al. and MacQueen et al. 1,30 The \mbox{CeO}_2 support was calcined in air at 600 °C for 3 h. The \mbox{ReO}_x was then impregnated on the \mbox{CeO}_2 via wet impregnation using an aqueous solution of ammonium perrhenate (NH4ReO4) while mixing the solution. The solution was dried at 110 °C for 12 h to ensure all the water has evaporated from the solution. The $\mbox{ReO}_x/\mbox{CeO}_2$ was then calcined in air at 500 °C for 3 h. Post calcination, the $\mbox{ReO}_x/\mbox{CeO}_2$ was then ground into powder using a mortar and pestle.

Raman Spectroscopy. The 1 wt % ReO_x/CeO₂ catalyst sample was subjected to in situ Raman spectroscopy. Initial scans were taken at room temperature in ambient air, with a Horiba XploRA Plus Raman microscope. The excitation source was a 30 mW, 638 nm diode laser, which was calibrated using a polystyrene standard. Scattered light was detected using a HORIBA Scientific charge-coupled device detector and thermoelectrically cooled to -50 °C. The sample was then heated to 550 °C at a rate of 50 °C/min while flowing 20 sccm ultra-high purity O₂ (99.9993% O₂) in a Linkam in situ Raman cell. Once at temperature, the samples were calcined for 30 min in the O_2 environment. Following the calcination, the O_2 environment was purged, and the samples were then reduced with 20 sccm H₂ at the same temperature for 10 min. The calcination and reduction treatments were repeated in cycles, and after the repeated reduction, the system was purged and sealed, and a 25 cm³ sample cylinder was attached to the cell with 2 bar of the ¹⁸O isotope. The ¹⁸O isotope was then introduced into the Linkam stage and the 1 wt % ReO_r/CeO₂ sample was calcined in the ¹⁸O environment for 30 min at 550 °C. The calcination temperature of 550 °C was based on the previous literature, which utilized calcination temperatures of 450-550 °C for isotopic ¹⁸O exchange. ^{11,12,31} The higher temperature allows for the faster kinetic exchange of the ¹⁸O and therefore ensures sufficient exchange within the time studied. The ReO_x/CeO₂ catalyst was then reduced again in the same H₂ conditions as prior and recalcined within the ¹⁸O isotope environment. Spectral measurements were taken after

each individual calcination and reduction treatment step and were baseline corrected before analysis.

Fourier Transform Infrared Spectroscopy. Additionally, the 1 wt % ReO_x/CeO₂ sample was subjected to in situ Fourier transform infrared spectroscopy (FTIR) as a complement to the information gathered from the in situ Raman spectroscopy. The in situ FTIR was taken at near identical conditions to the Raman spectroscopy. A Bruker Vertex 70 FTIR spectrometer equipped with an MCT detector and KBr beam splitter was used. The sample was placed in a diffuse reflectance infrared Fourier transform spectroscopy (DRIFTS) cell and was heated to 550 °C at 50 °C/min while flowing 20 sccm N₂. It was then calcined using a 25 cm³ sample cylinder that was attached to the DRIFTS cell with 20 psig ¹⁶O₂ for 30 min. Afterward, the sample was reduced with 20 sccm H₂ for 30 min. After purging the lines with N_2 , a sample cylinder filled with 20 psig $^{18}O_2$ was attached for the isotope exchange, and time-resolved measurements were taken for 30 min.

Catalyst Characterization. The ReO_x/CeO₂ catalyst was characterized using X-ray Diffraction (XRD), Brunauer-Emmett-Teller (BET) surface area analysis, inductively coupled plasma optical emission spectroscopy (ICP-OES), and temperature-programmed reduction (TPR). XRD patterns were collected using a Rigaku Miniflex II (Rigaku, Japan) using a Cu K α radiation source scanning from 20–80° 2 θ at a rate of 0.5° /min and a step size of 0.02° . The obtained pattern, see Figure 1S, matches reference patterns for CeO₂ with no peaks corresponding to any Re containing phase or other unidentified materials. BET surface area measurements were conducted using an ASAP 2020 (Micromeritics, USA) with nitrogen as the adsorbate gas. Surface area calculations were based upon a BET isotherm. The ceria support as provided by the manufacturer (Daiichi, Japan) without further treatment had a BET surface area of 84.7 m²/g, while the prepared catalyst had a surface area of 78.3 m²/g, with an instrumental error of $\pm 3.2 \text{ m}^2/\text{g}$. These values are in close agreement with each other and suggest that that the catalyst preparation methodology does not greatly impact the physical properties of the supporting ceria. ICP-OES was conducted by adding ~50 mg of catalyst to aqua regia and digesting for 8 h at 120 °C. A 1000 ppm ammonium perrhenate standard was utilized to construct calibration curves (Ricca Chemical Company, USA). An Avio 200 (PerkinElmer, USA) equipped with an S10 autosampler was utilized for data collection. The untreated 1 wt % nominal Re catalyst had an actual weight loading of 1.02 \pm 0.01 wt % Re and had a weight loading of 1.08 \pm 0.01 wt % after heat treating, attributable to the experimental error. A previous batch of catalyst had a Re loading of 1.02 ± 0.02 wt %, indicating good agreement between batches and excellent reproducibility with the catalyst synthesis technique. The number of Re atoms per nm² was determined to be 0.422 ± 0.002 atoms/nm² based on the ICP-OES and BET results. Reducibility of the catalyst was investigated via TPR using an AutoChem II 2920 (Micromeritics, USA) with an analysis gas consisting of 10% H2 balanced in Argon. Experiments were carried out using a ramp rate of 5 °C/min and an analysis gas flow rate of 50 sccm. Quantitative hydrogen uptake was calculated utilizing a three-point calibration with known quantities of silver(II) oxide (Micromeritics, USA). To ensure accuracy, experiments were repeated in triplicate, yielding a hydrogen uptake of 0.544 ± 0.037 mmol/g catalyst with a main reduction event with a maximum at ~408 °C, see Figure 2S. Metal loading on the catalyst is approximately 0.056 \pm

0.001 mmol Re/g catalyst indicating a higher than stoichiometric hydrogen uptake even with Re existing in the highest feasible oxidation state. Therefore, this excess hydrogen uptake may be attributable to interactions and hydrogen spillover with the supporting ceria. ¹

■ RESULTS/DISCUSSION

Isotopic ¹⁸O Exchange Raman Spectroscopy. The isotopic ¹⁸O Raman spectra were collected with two ¹⁸O exposure cycles following calcination cycles in ¹⁶O to ensure sufficient isotope exchange. ^{12,18} Each spectrum was normalized to the total area under its curve after baseline correction so that the spectrum had a total area of one. ^{32,33} Figure 2 shows the normalized spectra of a 1 wt % ReO_x/CeO₂ catalyst after the sample was exposed to each oxidation step during the isotope exchange experiment.

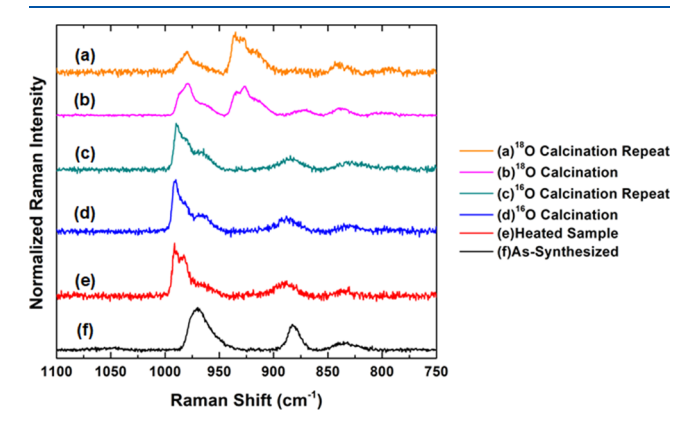


Figure 2. In situ Raman spectra. The heated sample, (e), was taken at 550 C in an Ar environment. The calcined sample spectra, (a-d), were obtained at 550 °C in the labeled gas environment.

The as-synthesized ReO_x/CeO₂ sample, seen in Figure 2f, shows three distinct bands, a convolution of the symmetric and asymmetric stretches of ${}^{16}O = Re = {}^{16}O$ (972 and 961 cm⁻¹), the asymmetric stretch of Re-16O-Re (881 cm-1), and the bending of Re-¹⁶OH (834 cm⁻¹) respectively, which will be further discussed below. Heating the samples in Ar at 550 °C resulted in shifting and splitting of the ReO, band (between 950 and 1000 cm⁻¹), revealing the presence of the mono-oxo species in addition to the di-oxo ReO_x species, seen in Figure 2e. After the reduction and recalcination of the samples, the band separation becomes more distinct, which is visible in Figure 2c,d. No new chemical species were observed; the current species are more pronounced in the spectrum. Once ¹⁸O isotope exchange occurs, new bands begin to appear at lower wavenumbers (between 900 and 950 cm⁻¹), shown in Figure 2b, due to the red shift caused by the increase in mass.³⁴ Upon repeat heating in an ¹⁸O environment, as seen in Figure 2a, the ¹⁶O band intensities decrease, and the intensities of the red-shifted bands associated with ¹⁸O begin to increase to levels similar to the heated samples, as seen in Figure 2e, indicating the ¹⁸O exchange. The difference in the signal-tonoise ratio (SNR) between Figure 2a (SNR = 12.0) and 2b (SNR = 31.8) was most likely due to slight variations in sample positions due to the experimental setup, not from the volatility of ReO_x. This has been verified in the ICP where Re weight loading before heating was 1.01 \pm 0.01 wt % and after heating was 1.08 ± 0.01 wt %. The sample cylinder containing the isotope oxygen required manual replacement during the experiment, which resulted in slight positional changes of the sample. However, it can be reasonably assumed that the ${\rm ReO}_x$ distribution across the ${\rm CeO}_2$ is constant. Additionally, the supplemental Figure 3S shows a set of Raman spectra of the sample that has been unperturbed before and after calcination at 550 °C. The SNR, with respect to the band at 989 cm⁻¹, decreased from 51.5 to 45.3 after heating for 3 h.

Further inspection of the as-synthesized sample (Figure 2f) shows that the highest wavenumber bands can be deconvoluted into two bands, as seen in Figure 3. These bands are

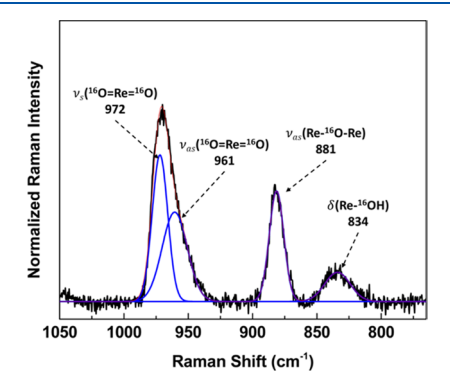


Figure 3. As-synthesized 1 wt % ReO_x/CeO₂ Raman spectrum at ambient conditions.

fitted to 972 and 961 cm⁻¹ wavenumbers with a Gaussian band shape³⁵ and were identified as the symmetric di-oxo and asymmetric di-oxo stretch, respectively. The di-oxo ReO_x species present in the as-synthesized sample supports the reaction mechanism proposed by Ota et al. due to the presence of the proposed surface species. Additionally, the

spectrum shows a band at 881 cm⁻¹, which is indicative of the asymmetric stretch of the oxygen bridge between two rhenium atoms. 21 This oxygen bridge corresponds to a cross-linked ReO_x species, which has previously been proposed as inactive for S-HDO.¹ A final band at 834 cm⁻¹ shows the in-plane bending of a hydroxyl group attached to the rhenium.²¹ In order to verify the presence of the hydroxyl species, additional spectra were taken at regions where the O-H vibration is present. While the known Re-OH stretch at 700 cm⁻¹ was not observed in the Raman, a low-intensity band is observed at the 3700 cm⁻¹ Raman spectral region where O-H is visible, seen in Figure 4S.²¹ The terminal hydroxyl group is likely attached to the Re in a mono-oxo structure, as previously proposed by Xi et al.² The hydroxylated structure has not been proposed as a starting structure in a reaction mechanism. However, the hydroxylated structures can be reduced and the mono-oxo structures regenerated through a hydrogen migration process, which facilitates catalyst regeneration in the Xi et al. mechanism.² Thus, the hydroxylated species could still play a role in the S-HDO reaction when hydrogen is present to allow the reduction and regeneration of the ReO_x species.

The presence of multiple species within the spectrum of the as-synthesized sample shows that there is not a singular configuration for ReO_x. This was also observed in previous works studying a ReO_x/TiO₂ catalyst¹⁹ and with previous work done by Wachs et al. on ReO_x on various metal oxide supports excluding CeO₂. ^{13,18,36} The various ReO_x species present could have their own respective S-HDO reaction mechanisms. However, it is not possible to discern which species is dominating in the reaction or which species are participating in the reaction without further studies into Re coverage effects and respective reaction data. The formation of hydroxyl groups

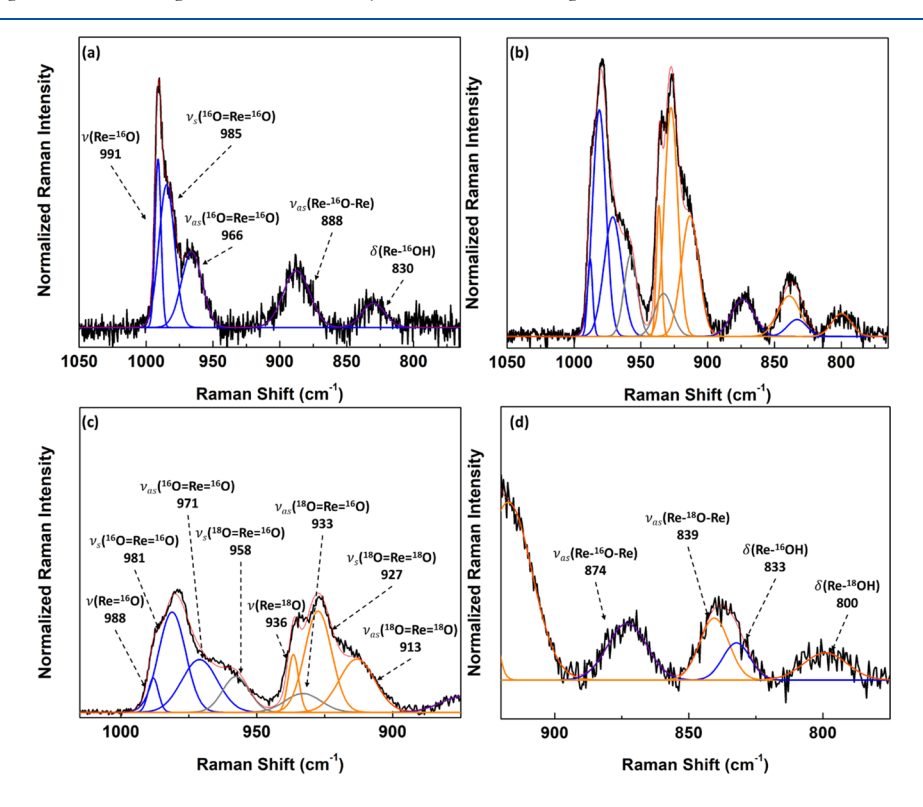


Figure 4. Raman spectra of 1.0 wt % ReO_x/CeO_2 after the first isotope exchange at 550 °C. (a) Heated sample calcined in flowing $^{16}O_2$ before the exchange. (b) Heated sample calcined in $^{18}O_2$. (c) Fitting and identification of the mono and di-oxo configurations. 19 (d) Fitting and identification of the bridge and hydroxyl group bands.

on the surface has not been typically seen in the experimental literature but has been theorized through DFT.² While the DFT showed that hydroxyl groups can be favorable to form, only a low-intensity bending mode between Re and OH can be observed in our spectra at 834 cm⁻¹. Since the hydroxyl groups are likely reduced and removed through a hydrogen migration process under the reducing reaction conditions, ^{1,2} it should be unlikely to see these structures in a high concentration on the surface during reaction or under a reaction environment.

At elevated temperatures, a third band appears adjacent to the bands previously centered around 972 and 961 cm⁻¹, as seen in Figure 2e. Figure 4 shows a comparison between the sample calcined in $^{16}\mathrm{O}_2$ and the calcination of the sample in $^{18}\mathrm{O}_2$ isotope conditions. From this spectrum, we can see four different ReO_x species present within the sample: the monooxo structure, di-oxo structure, cross-linked bridge, and hydroxyl bond.

The red shift observed in the Raman spectra before and after isotope exchange seen in Figure 4 confirms the four different surface configurations of ReO_x . Notably, the region for the ReO_x bands that correspond with the rhenium and oxygen double bond stretches shows spectroscopic evidence for two separate configurations. Before the isotope exchange, a band at 991 cm⁻¹ is identified with a mono-oxo termination configuration ($\text{Re}=^{16}\text{O}$), see Figure 5b. The mono-oxo

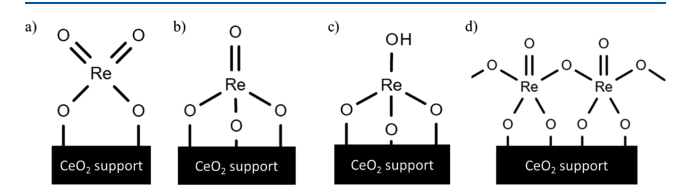


Figure 5. ReO_x species present on the surface of ReO_x/CeO₂. (a) Dioxo species. (b) Mono-oxo species. (c) Hydroxyl species. (d) Crosslinked Re species.

ReO_x is the most stable and energetically favorable structure according to the calculations performed by Xi et al² The bands at 985 and 966 cm⁻¹ relate to the symmetric and asymmetric stretches, respectively, of the di-oxo termination of ReO_x (¹⁶O=Re=¹⁶O), see Figure 5a. The di-oxo structure is the active site proposed in the calculations performed by Ota et al¹ Additionally, the asymmetric stretch for the oxygen bridge between rhenium metal atoms (Re-¹⁶O-Re) can be seen at 888 cm⁻¹, see Figure 5d, and the in-plane bending of the hydroxyl group (Re-¹⁶OH) is labeled at 830 cm⁻¹, see Figure 5c. The di-oxo, mono-oxo, and hydroxyl Re species that form are isolated monomeric species, see Figure 5a-c. However, when the cross-linked Re species is formed, see Figure 5d, it forms an oligomeric Re species.

After a single oxidation in ¹⁸O isotope, exchange can be seen for each configuration present. The mono-oxo termination configuration is red-shifted by 52 to 936 cm⁻¹, and the bridge and hydroxyl oxygens are similarly shifted to lower wavenumbers at 839 and 800 cm⁻¹ respectively. When both ¹⁶O are exchanged with ¹⁸O in the di-oxo structure (¹⁸O=Re=¹⁸O), the stretches are clearly visible at 927 cm⁻¹ for the symmetric stretch and 913 cm⁻¹ for the asymmetric stretch. However, the bands for the single isotope exchange for the same stretches (¹⁶O=Re=¹⁸O) were deconvoluted via fitting their locations based on their theoretical positions seen in Table 1. This provided a better fit for all the spectra and allowed for position

Table 1. Experimental and Theoretical Raman Shift for the Isotope Exchange

Raman shifts (cm ⁻¹)				
	¹⁸ O ₂ theoretical		¹⁸ O ₂ measured	
vibrational mode	single sub	double sub	single sub	double sub
ν (Re=O)	939	N/A	936	N/A
ν_s (O=Re=O)	955	933	958	927
ν_{as} (O=Re=O)	937	915	933	913
v_{as} (Re-O-Re)	841	N/A	839	N/A
δ (Re–OH)	786	N/A	800	N/A

identification of the single exchanged symmetric stretch to be at 958 cm $^{-1}$ and the asymmetric stretch to be at 933 cm $^{-1}$. All instances of band fitting were performed with proper constraints to the full-width at half-maximum of the Raman bands of the same species and a constraint to the area ratio of the symmetric and asymmetric stretches of the di-oxo ${\rm ReO}_x$ bands.

Using the model for a simple rigid diatomic molecule, theoretical vibrational frequency ratios can be estimated for an isotope exchange. This isotopic ratio can be determined using the following expression: 11,34,37,38

$$\frac{\nu_{^{16}\text{O}}}{\nu_{^{18}\text{O}}} = \sqrt{\frac{\frac{1}{\text{m}_{\text{M}}} + \frac{1}{\text{m}_{^{16}\text{O}}}}{\frac{1}{\text{m}_{\text{M}}} + \frac{1}{\text{m}_{^{18}\text{O}}}}} \approx \sqrt{\frac{m_{^{18}\text{O}}}{m_{^{16}\text{O}}}}, m_{\text{M}} \gg m_{^{16}\text{O}}, m_{^{18}\text{O}}$$

where the vibrational frequencies of metal-16O and metal-18O isotope bond are represented by ν_{160} and ν_{180} , respectively. The atomic mass of the metal is $m_{\mathrm{M}\nu}$ and those of the oxygen and isotope are m_{160} and m_{180} , respectively. When the mass of the metal is much greater than the mass of the oxygen atoms, the equation can be simplified to the square root of the ratio between the mass of the ¹⁸O and the mass of the ¹⁶O. Typically, the diatomic model would only be used for monooxo constituents. However, it has been used before on the isotope exchange of the di-oxo speciation of Cr₂O₃/SiO₂ and on CaCO₂. 18,37 This model has been used as a first approximation to estimate the red shift from bond vibration dampening effect by the increase in mass. A more accurate theoretical estimate would require first principle computational techniques that are outside the scope of this work. Table 1 shows the theoretical vibrational shift versus the experimental shift. The measured values are consistent with the theoretically calculated shift. The average difference in the red shift from the vibrational stretches was 3.16 cm⁻¹.

The isotope exchange ratio can be seen in Table 1S and is determined by the fitted area of the bands that indicate single-and double-substituted modes divided by the fitted area of the unsubstituted ReO_x bands. After the initial exposure to $^{18}\rm{O}$, each species experienced at least 50% isotope exchange, which can be seen with the $^{18}\rm{O}-^{16}\rm{O}$ ratio being greater than 1 for each species. The mono-oxo ReO_x species has the highest exchange efficiency, with an exchange of approximately 62%. After an additional cycle, the mono-oxo species was 90% exchanged, and the di-oxo species was 70% exchanged. Interestingly, the cross-linked and hydroxyl species exchange to near completion, with the $^{16}\rm{O}$ bands no longer visible within the spectra. The higher extent of exchange of the mono-oxo species, as compared to the di-oxo species, suggests that the mono-oxo ReO_x species is more reactive toward oxygen in

the gas phase. This makes a shift in the oxidation state more likely to occur for the mono-oxo as compared to the di-oxo ReO_x species.

Isotopic ¹⁸O **DRIFTS.** Fourier transform infrared spectroscopy was employed to provide a time resolved observation of the band formation from the isotope exchange. For Figure 6,

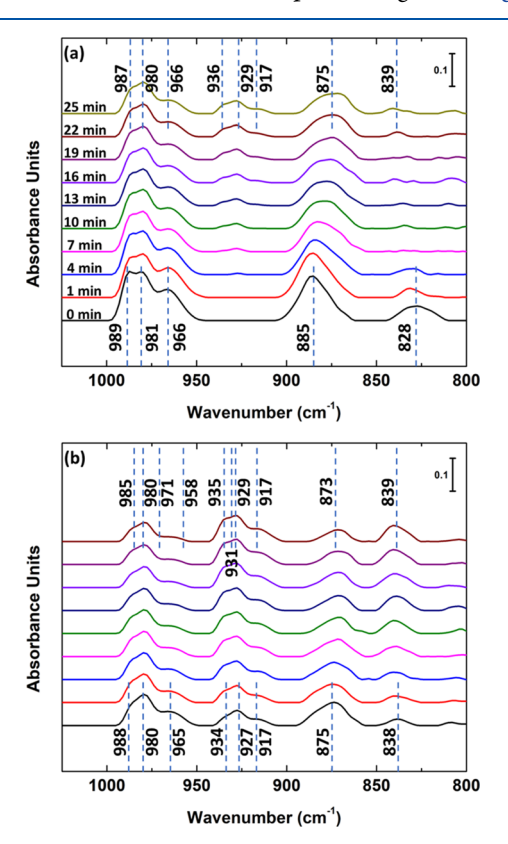


Figure 6. Time-resolved FTIR spectra of reduced 1 wt % ReO_x/CeO_2 exposed to ^{18}O . (a) Sample was exposed to ^{18}O after reduction. (b) Sample was reintroduced to ^{18}O after a second reduction.

the experiment was started with the 1 wt % ReO../CeO. sample surface oxidized with ¹⁶O. The sample was then exposed to the ¹⁸O isotope at 550 °C for 25 min, which was repeated for a second cycle. The data complements the Raman spectra and shows the redshift of the Re=O and bridge vibrations. However, it is difficult to observe the hydroxyl isotope band formation as the adsorption of the ¹⁸O occurs, which is potentially due to the low intensity of the Re-OH bending mode.²¹ Additionally, initial analysis of the band intensities would imply that the asymmetric stretch of the dioxo species is less than the intensity of the symmetric stretch, which violates the selection rules for IR. However, when accounting for the integrated intensity, we have found that the fitted area is near equivalent or greater than the integrated intensity of the symmetric stretch. Therefore, the selection rule has been satisfied.³⁹⁻⁴³ Table 3S shows the integrated area comparisons of the symmetric and asymmetric stretches of the di-oxo species for Raman and FTIR spectroscopies, respectively.

With the time resolved measurements, we can observe the amount of isotope that is exchanged per reduction and oxidation cycle. After about 15 min of exposure to the isotope at 550 °C, the exchange reaches a steady state. The amount of actual exchange can be determined using the ratio of the band

area of the ¹⁸O sample and the band area of the ¹⁶O sample. The spectra used after the second cycle of the isotope exchange were used to calculate band areas. After two cycles of ¹⁸O exposure, the area ratios show a similar trend in the change done to the ReO, that was seen in the Raman spectra, as shown in Table 2S. After 25 min, 60.5% of the ¹⁶O in the sample was exchanged with ¹⁸O, and the ratio of ¹⁸O/¹⁶O was 1.534. Before reaching the steady state, the ¹⁸O/¹⁶O exchange rate was linear and was calculated based on the 1, 7, and 13 min spectra. The ¹⁸O/¹⁶O exchange rate was calculated to be 2.29% per minute, with the ${}^{18}O/{}^{16}O$ ratios being 0.308, 0.546, and 1.043 for the 1, 7, and 13 min spectra, respectively. The symmetric and asymmetric di-oxo stretches and the bridge band show further exchange in the IR, but the mono-oxo stretch shows less exchange than in a single exposure in the Raman. However, this could simply be a result of a different measurement technique used in the analysis. The ratios of ¹⁸O exchange for the IR results in differences are not nearly as drastic as seen in the Raman. The relative similarity in the mono-oxo and di-oxo 18O/16O exchange ratios relative to the Raman supports that the species might be more similar in their ability to react with the environment.

CONCLUSIONS

Using in situ 18 O isotopic exchange Raman spectroscopy and DRIFTS, the structures of ReO_x supported on CeO_2 have been determined to be di-oxo (O=Re=O), mono-oxo (Re=O), cross-linked (Re-O-Re), and mono-oxo with a hydroxyl group (Re-OH) via their respective red-shifted bands. The Raman and IR data showed that the extent of exchange after cycling 18 O was approximately 60%, while the time resolved IR showed that the 18 O/ 16 O exchange rate was 2.29% per minute. Our results show that there are multiple structures of ReO_x present when supported CeO_2 .

ASSOCIATED CONTENT

5 Supporting Information

The Supporting Information is available free of charge at https://pubs.acs.org/doi/10.1021/acs.jpcc.9b11338.

XRD pattern of 1 wt % ReO_x/CeO_2 , TPR spectrum of 1 wt %, Raman O–H stretching region at a higher Raman shift, signal-to-noise comparison between ambient and heated Raman spectra, ReO_x/CeO_2 , Raman $^{18}O/^{16}O$ band area ratios, FTIR $^{18}O/^{16}O$ band area ratios, and symmetric to asymmetric di-oxo band ratios for Raman and FTIR spectroscopies (PDF)

AUTHOR INFORMATION

Corresponding Author

Jochen Lauterbach — Department of Chemical Engineering, University of South Carolina, Columbia, South Carolina 29208, United States; ⊙ orcid.org/0000-0001-8303-7703; Email: lauteraj@cec.sc.edu

Authors

Blake MacQueen – Department of Chemical Engineering, University of South Carolina, Columbia, South Carolina 29208, United States

Benjamin Ruiz-Yi — Department of Chemical Engineering, University of South Carolina, Columbia, South Carolina 29208, United States

- Michael Royko Department of Chemical Engineering, University of South Carolina, Columbia, South Carolina 29208, United States
- Andreas Heyden Department of Chemical Engineering, University of South Carolina, Columbia, South Carolina 29208, United States; oorcid.org/0000-0002-4939-7489
- Yomaira J. Pagan-Torres Department of Chemical Engineering, University of Puerto Rico-Mayaguez Campus, Mayaguez, Puerto Rico 00681-9000, United States
- Christopher Williams Department of Chemical Engineering, University of South Carolina, Columbia, South Carolina 29208, United States; orcid.org/0000-0002-4012-5364

Complete contact information is available at: https://pubs.acs.org/10.1021/acs.jpcc.9b11338

Notes

The authors declare no competing financial interest.

ACKNOWLEDGMENTS

We gratefully acknowledge financial support from the National Science Foundation (OIA-1632824 and DGE-1250052). This work was also supported by the South Carolina Smart State Center for Strategic Approaches to the Generation of Electricity (SAGE). We would like to acknowledge Elizabeth Barrow for the scientific discussion and Savannah Howell for the assistance with the ICP-OES experimentation.

REFERENCES

- (1) Ota, N.; Tamura, M.; Nakagawa, Y.; Okumura, K.; Tomishige, K. Performance, Structure, and Mechanism of ReO_x-Pd/CeO₂ Catalyst for Simultaneous Removal of Vicinal OH Groups with H₂. ACS Catal. **2016**, *6*, 3213–3226.
- (2) Xi, Y.; Yang, W.; Ammal, S. C.; Lauterbach, J.; Pagan-Torres, Y.; Heyden, A. Mechanistic Study of the Ceria Supported, Re-Catalyzed Deoxydehydration of Vicinal OH Groups. *Catal. Sci. Technol.* **2018**, *8*, 5750–5762.
- (3) Wachs, I. E. Raman and IR Studies of Surface Metal Oxide Species on Oxide Supports: Supported Metal Oxide Catalysts. *Catal. Today* **1996**, *27*, 437–455.
- (4) Gómez-Cortés, A.; Márquez, Y.; Arenas-Alatorre, J.; Díaz, G. Selective CO Oxidation in Excess of H₂ over High-Surface Area CuO/CeO₂ Catalysts. *Catal. Today* **2008**, *133-135*, 743–749.
- (5) Bumajdad, A.; Zaki, M. I.; Eastoe, J.; Pasupulety, L. Microemulsion-Based Synthesis of CeO₂ Powders with High Surface Area and High-Temperature Stabilities. *Langmuir* **2004**, *20*, 11223–11233
- (6) Li, H. F.; Zhang, N.; Chen, P.; Luo, M. F.; Lu, J. Q. High Surface Area Au/CeO₂ Catalysts for Low Temperature Formaldehyde Oxidation. Appl. Catal. B Environ. 2011, 110, 279–285.
- (7) Luo, M. F.; Song, Y. P.; Lu, J. Q.; Wang, X. Y.; Pu, Z. Y. Identification of CuO Species in High Surface Area CuO-CeO₂ Catalysts and Their Catalytic Activities for CO Oxidation. *J. Phys. Chem. C* **2007**, *111*, 12686–12692.
- (8) Periyat, P.; Laffir, F.; Tofail, S. A. M.; Magner, E. A Facile Aqueous Sol-Gel Method for High Surface Area Nanocrystalline CeO₂. RSC Adv. **2011**, *1*, 1794–1798.
- (9) Kašpar, J.; Fornasiero, P.; Graziani, M. Use of CeO₂-Based Oxides in the Three-Way Catalysis. *Catal. Today* **1999**, *50*, 285–298.
- (10) Tang, X.; Zhang, B.; Li, Y.; Xu, Y.; Xin, Q.; Shen, W. Carbon Monoxide Oxidation over CuO/CeO₂ Catalysts. *Catal. Today* **2004**, 93-95, 191–198.
- (11) Weckhuysen, B. M.; Jehng, J.-M.; Wachs, I. E. In Situ Raman Spectroscopy of Supported Transition Metal Oxide Catalysts: ¹⁸O₂–¹⁶O₂ Isotopic Labeling Studies. *J. Phys. Chem. B* **2000**, *104*, 7382–7387.

- (12) Weckhuysen, B. M.; Wachs, I. E. *In Situ* Raman Spectroscopy of Supported Chromium Oxide Catalysts: ¹⁸O₂–¹⁶O₂ Isotopic Labeling Studies. *J. Phys. Chem. B* **1997**, *101*, 2793–2796.
- (13) Wachs, I. E.; Roberts, C. A. Monitoring Surface Metal Oxide Catalytic Active Sites with Raman Spectroscopy. *Chem. Soc. Rev.* **2010**, *39*, 5002–5017.
- (14) Wu, Z.; Dai, S.; Overbury, S. H. Multiwavelength Raman Spectroscopic Study of Silica-Supported Vanadium Oxide Catalysts. *J. Phys. Chem. C* **2010**, *114*, 412–422.
- (15) Wu, Z.; Rondinone, A. J.; Ivanov, I. N.; Overbury, S. H. Structure of Vanadium Oxide Supported on Ceria by Multiwavelength Raman Spectroscopy. *J. Phys. Chem. C* **2011**, *115*, 25368–25378.
- (16) Tsilomelekis, G.; Boghosian, S. In Situ Raman and FTIR Spectroscopy of Molybdenum(VI) Oxide Supported on Titania Combined with ¹⁸O/¹⁶O Exchange: Molecular Structure, Vibrational Properties, and Vibrational Isotope Effects. *J. Phys. Chem. C* **2010**, 115, 2146–2154.
- (17) Lwin, S.; Keturakis, C.; Handzlik, J.; Sautet, P.; Li, Y.; Frenkel, A. I.; Wachs, I. E. Surface ReOx Sites on Al_2O_3 and Their Molecular Structure-Reactivity Relationships for Olefin Metathesis. *ACS Catal.* **2015**, *5*, 1432–1444.
- (18) Lee, E. L.; Wachs, I. E. In Situ Raman Spectroscopy of SiO₂-Supported Transition Metal Oxide Catalysts: An Isotopic ¹⁸O-¹⁶O Exchange Study. *J. Phys. Chem. C* **2008**, *112*, 6487–6498.
- (19) Andriopoulou, C.; Boghosian, S. Molecular Structure and Termination Configuration of Oxo-Re(VII) Catalyst Sites Supported on Titania. *Catal. Today* **2019**, DOI: 10.1016/j.cattod.2019.06.054.
- (20) Andriopoulou, C.; Anastasiou, I.; Boghosian, S. Di-Oxo and Tri-Oxo Re(VII)-Oxosulfato Complexes in the Re₂O₇-K₂S₂O₇ Molten System. Molecular Structure, Vibrational Properties and Temperature-Dependent Interconversion. *Vib. Spectrosc.* **2019**, *100*, 14–21.
- (21) Beattie, I. R.; Gilson, T. R.; Jones, P. J. Vapor Phase Vibrational Spectra for Re₂O₇ and the Infrared Spectrum of Gaseous HReO₄. Molecular Shapes of Mn₂O₇, Tc₂O₇, and Re₂O₇. *Inorg. Chem.* **1996**, 35, 1301–1304.
- (22) Tazawa, S.; Ota, N.; Tamura, M.; Nakagawa, Y.; Okumura, K.; Tomishige, K. Deoxydehydration with Molecular Hydrogen over Ceria-Supported Rhenium Catalyst with Gold Promoter. *ACS Catal.* **2016**, *6*, 6393–6397.
- (23) Nakagawa, Y.; Tazawa, S.; Wang, T.; Tamura, M.; Hiyoshi, N.; Okumura, K.; Tomishige, K. Mechanistic Study of Hydrogen-Driven Deoxydehydration over Ceria-Supported Rhenium Catalyst Promoted by Au Nanoparticles. *ACS Catal.* **2018**, *8*, 584–595.
- (24) Wang, T.; Liu, S.; Tamura, M.; Nakagawa, Y.; Hiyoshi, N.; Tomishige, K. One-Pot Catalytic Selective Synthesis of 1,4-Butanediol from 1,4-Anhydroerythritol and Hydrogen. *Green Chem.* **2018**, 20, 2547–2557.
- (25) Tamura, M.; Yuasa, N.; Cao, J.; Nakagawa, Y.; Tomishige, K. Transformation of Sugars into Chiral Polyols over a Heterogeneous Catalyst. *Angew. Chem., Int. Ed.* **2018**, *57*, 8058–8062.
- (26) Cao, J.; Tamura, M.; Nakagawa, Y.; Tomishige, K. Direct Synthesis of Unsaturated Sugars from Methyl Glycosides. *ACS Catal.* **2019**, *9*, 3725–3729.
- (27) Wang, T.; Tamura, M.; Nakagawa, Y.; Tomishige, K. Preparation of Highly Active Monometallic Rhenium Catalysts for Selective Synthesis of 1,4-Butanediol from 1,4-Anhydroerythritol. *ChemSusChem* **2019**, *12*, 3615–3626.
- (28) Donnelly, L. J.; Thomas, S. P.; Love, J. B. Recent Advances in the Deoxydehydration of Vicinal Diols and Polyols. *Chem. Asian J.* **2019**, *14*, 3782–3790.
- (29) Ota, N.; Tamura, M.; Nakagawa, Y.; Okumura, K.; Tomishige, K. Hydrodeoxygenation of Vicinal OH Groups over Heterogeneous Rhenium Catalyst Promoted by Palladium and Ceria Support. *Angew. Chem., Int. Ed.* **2015**, *54*, 1897–1900.
- (30) MacQueen, B.; Barrow, E.; Rivera Castro, G.; Pagan-Torres, Y.; Heyden, A.; Lauterbach, J. Optimum Reaction Conditions for 1,4-Anhydroerythritol and Xylitol Hydrodeoxygenation over a ReO_x-Pd/CeO₂Catalyst via Design of Experiments. *Ind. Eng. Chem. Res.* **2019**, 58, 8681–8689.

- (31) Vuurman, M. A.; Wachs, I. E. In Situ Raman Spectroscopy of Alumina-Supported Metal Oxide Catalysts. *J. Phys. Chem.* **1992**, *96*, 5008–5016.
- (32) Andriopoulou, C.; Boghosian, S. Tuning the Configuration of Dispersed Oxometallic Sites in Supported Transition Metal Oxide Catalysts: A Temperature Dependent Raman Study. *Catal. Today* **2019**, 336, 74–83.
- (33) Barrow, E. Heterogeneous Catalysis for the Upgrading of Biomass Derived Chemicals via Hydrodeoxygenation. Ph.D. Dissertation, University of South Carolina, Columbia, SC, 2019.
- (34) Zhang, P. X.; Huang, S. J.; Habermeier, H. U.; Zhao, G. M. Isotope Effect on Raman Spectra of Polycrystalline La_{0.67}Ca_{0.33}MnO₃. *J. Raman Spectrosc.* **2001**, 32, 812–816.
- (35) Bradley, M. S.; Bratu, C. Vibrational Line Profiles as a Probe of Molecular Interactions. *J. Chem. Educ.* **1997**, *74*, 553–555.
- (36) Kim, D. S.; Wachs, I. E. Surface Rhenium Oxide-Support Interaction for Supported Re2O7 Catalysts. *J. Catal.* **1993**, *141*, 419–429.
- (37) Gillet, P.; McMillan, P.; Schott, J.; Badro, J.; Grzechnik, A. Thermodynamic Properties and Isotopic Fractionation of Calcite from Vibrational Spectroscopy of 18O-Substituted Calcite. *Geochim. Cosmochim. Acta* 1996, 60, 3471–3485.
- (38) Tsilomelekis, G.; Boghosian, S. In Situ Raman and FTIR Spectroscopy of Molybdenum(VI) Oxide Supported on Titania Combined with ¹⁸O/¹⁶O Exchange: Molecular Structure, Vibrational Properties, and Vibrational Isotope Effects. *J. Phys. Chem. C* **2010**, *115*, 2146–2154.
- (39) Wexler, A. S. Integrated Intensities of Absorption Bands in Infrared Spectroscopy. *Appl. Spectrosc. Rev.* **1967**, *1*, 29–98.
- (40) Painter, P. C.; Snyder, R. W.; Starsinic, M.; Coleman, M. M.; Kuehn, D. W.; Davis, A. Concerning the Application of Ft-Ir To the Study of Coal: A Critical Assessment of Band Assignments and the Application of Spectral Analysis Programs. *Appl. Spectrosc.* **2016**, *35*, 475–485.
- (41) Fan, J.; Trenary, M. Symmetry and the Surface Infrared Selection Rule for the Determination of the Structure of Molecules on Metal Surfaces. *Langmuir* **1994**, *10*, 3649–3657.
- (42) Snyder, R. G.; Hsu, S. L.; Krimm, S. Vibrational Spectra in the C H Stretching Region and the Structure of the Polymethylene Chain. *Spectrochim. Acta Part A* **1978**, *34*, 395–406.
- (43) Hagemann, H.; Snyder, R. G.; Peacock, A. J.; Mandelkern, L. Quantitative Infrared Methods for the Measurement of Crystallinity and Its Temperature Dependence Polyethylene. *Macromolecules* **1989**, 22, 3600–3606.